Clinical Proteomics

RESEARCH

Open Access

Histology-resolved proteomics reveals distinct tumor and stromal profiles in low- and high-grade prostate cancer

Allison L. Hunt[1,2], Waleed Barakat[2,3,4], Sasha C. Makohon-Moore[2,3,4], Brian L. Hood[2,3,4], Kelly A. Conrads[2,3,4], Katlin N. Wilson[2,3,4], Tamara Abulez[2,3,4], Jonathan Ogata[2,3,4], Kenneth J. Pienta[5], Tamara L. Lotan[6,7,8], Haresh Mani[9], Donald L. Trump[10], Nicholas W. Bateman[2,3,4] and Thomas P. Conrads[1,2,4*]

Abstract

Background Prostate cancer is one of the most frequently diagnosed cancers in men. Prostate tumor staging and disease aggressiveness are evaluated based on the Gleason scoring system, which is further used to direct clinical intervention. The Gleason scoring system provides an estimate of tumor aggressiveness through quantitation of the serum level of prostate specific antigen (PSA) and histologic assessment of Grade Group, determined by the Gleason Grade of the tumor specimen.

Methods To improve our understanding of the proteomic characteristics differentiating low- versus high-grade prostate cancer tumors, we performed a deep proteomic characterization of laser microdissected epithelial and stromal subpopulations from surgically resected tissue specimens from patients with Gleason 6 (n = 23 specimens from n = 15 patients) and Gleason 9 (n = 15 specimens from n = 15 patients) prostate cancer via quantitative high-resolution liquid chromatography-tandem mass spectrometry analysis.

Results In total, 789 and 295 grade-specific significantly altered proteins were quantified in the tumor epithelium and tumor-involved stroma, respectively. Benign epithelial and stromal populations were not inherently different between Gleason 6 versus Gleason 9 specimens. Notably, 598 proteins were exclusively significantly altered between Gleason 9 (but not Gleason 6) tumor-involved stroma and benign stroma, including several proteins involved in cholesterol biosynthesis and nucleotide metabolism.

Conclusions Proteomic alterations between Gleason 6 versus Gleason 9 were exclusive to the disease microenvironment, observed in both the tumor epithelium and tumor-involved stroma. Further, the molecular alterations measured in the tumor-involved stroma from Gleason 9 cases relative to the benign stroma have unique significance in disease aggressiveness, development, and/or progression. Our data provide supportive evidence of a need for further investigations into targeting stromal reservoirs of cholesterol and/or deoxynucleoside triphosphates in PCa tumors and further highlight the necessity for independent examination of the TME epithelial and stromal compartments.

Keywords Prostate cancer, Proteomics, Laser microdissection, Tumor microenvironment

*Correspondence:
Thomas P. Conrads
thomas.conrads@inova.org
Full list of author information is available at the end of the article

Background

Prostate cancer (PCa) is one of the most common cancers diagnosed in men, with 313,780 new cases and 35,770 deaths predicted to occur in the United States in 2025 [1]. Staging of PCa employing the American Joint Commission on Cancer TNM system depends on a description of tumor extent (TNM) and Gleason Grade Group (GG), and serum prostate specific antigen (PSA) quantitation [2, 3]. Assignment to a GG is determined by assessment of the extent of histologic abnormality of the two most dominant morphologies in the cancer specimen, with Gleason scores consisting of two individual scores [3] which are then summed to assign the GG. Tumors in GG 1 have low malignant potential and do not require immediate therapeutic intervention [2], whereas tumors in GG 5 have a high propensity for progression and spread.

Several previous studies have examined the proteogenomic differences between cellular subpopulations isolated from low- versus high-grade PCa tumors [4–8]. Prostatic stromal contributions toward malignant transformation and disease aggressiveness are widely appreciated, thus recent proposals have recommended grading the "reactive stroma" in addition to the classical Gleason scoring of the tumor epithelial component [9–11]. A marked phenotypic alteration in the tumor microenvironment (TME) occurs in which the normal prostatic stroma is predominated by smooth muscle cells with low abundances of fibroblasts, vascular cells, nerve cells, and infiltrating immune populations [12], whereas the tumor-transformed PCa stroma contains a high proportion of fibroblasts, extensive extracellular matrix remodeling, and an immunologically "cold" phenotype [7, 13].

To characterize proteomic drivers of aggressive PCa, we performed a deep proteomic characterization of laser microdissection (LMD) enriched epithelial and stromal subpopulations from low (Gleason 6) and high (Gleason 9) grade PCa tissue specimens using quantitative high-resolution liquid chromatography-tandem mass spectrometry (LC–MS/MS) analysis.

Methods

Tissue specimens

Surgically resected formalin-fixed paraffin-embedded (FFPE) tumor specimens (n = 38) were obtained from patients with PCa (n = 30) who underwent radical prostatectomy. An up-to-date evaluation of representative hematoxylin and eosin (H&E) stained sections from each specimen was performed using current International Society of Urological Pathology (ISUP) guidelines by a board-certified pathologist. Specific Gleason 6 or 9 regions of interest were annotated to inform LMD enrichment. All specimens were acinar adenocarcinomas; no foamy cell variants were included. All Gleason 6 specimens were scored as 3 + 3 = 6 (n = 23 specimens from n = 15 patients; 1–2 specimens/patient). All Gleason 9 specimens (n = 15 specimens from n = 15 patients) were scored as 4 + 5 = 9, with one exception (patient J4255, Gleason 5 + 4 = 9). Serial consecutive tissue thin Sects. (8 µm) were placed onto polyethylene napthalate (PEN) membrane slides (Leica Microsystems, Wetzlar, Germany) and H&E-stained prior to LMD.

Laser microdissection

Glandular tumor epithelium with associated intraluminal proteomic secretions (LMD enriched tumor; ET) was enriched using the LMD7 (Leica Microsystems). For the Gleason 9 tissue specimens, regions of Gleason 4 and Gleason 5 were collectively harvested into the sample collection tube for analysis. Areas containing high immune infiltration, necrosis, or blood were avoided. Benign epithelium (BE) was harvested when sufficiently present. Stroma surrounding the tumor and benign epithelium (tumor-involved stroma (ES) and benign stroma (BS), respectively) were additionally harvested when sufficiently present. Pre- and post-LMD micrographs were imaged using the Aperio ScanScope XT slide scanner (Leica Microsystems).

Liquid chromatography-tandem mass spectrometry

LMD-harvested samples were digested, quantitated, and labeled (10 µg peptide digest/sample) using isobaric tandem mass tags (TMT11, Thermo Fisher Scientific, Inc., Waltham, MA, USA), as previously described [14]. Two sets of TMT multiplexes were generated containing either the epithelial (ET and BE) samples (n = 6 multiplexes) or stromal (ES and BS) samples (n = 7 multiplexes). The multiplexes were fractionated by basic reversed-phase liquid chromatography (bRPLC), pooled into 24 concatenated fractions, and resuspended in 25 mM ammonium bicarbonate. Approximately 1.5 µg from each resuspended pooled fraction was analyzed by LC–MS/MS employing a nanoflow LC system (EASY-nLC 1200, Thermo Fisher Scientific, Inc.) coupled online with either an Orbitrap Fusion Lumos Tribrid MS (Thermo Fisher Scientific, Inc.) for the epithelial sample set, or a Q Exactive HF-X Orbitrap MS (Thermo Fisher Scientific, Inc.) for the stromal sample set, as previously described [15]. Protein-level roll-up was performed as previously described [14].

Bioinformatic and statistical analyses

Unsupervised hierarchical clustering was performed using 100 proteins with the highest median absolute deviation (MAD) across all samples and clustered using pheatmap (version 1.0.12) in R (version 4.3.2) using a "correlation" distance metric and "ward.D"

clustering. Differential analyses were performed using limma (version 3.58.1 [16]) in R. Proteins passing a limma adjusted (adj.) $p < 0.05$ were prioritized for downstream comparative and pathway analyses. Functional pathway annotation was performed using Ingenuity Pathway Analysis (IPA, Qiagen Sciences, LLC, Germantown, MD, USA). Specifically, analyses of alterations in ET versus BE were performed using the IPA "Spring release 2021". Analyses of alterations in ES versus BS was performed using IPA "Winter release 2023". Known or putative drug targets were cross-referenced against a list of 150 FDA-approved anticancer drugs reported by Sun et al. [17]. Spearman correlations were calculated co-altered proteins in each of the following datasets: our Gleason 6 versus 9 ET and Staunton et al. Table S1.3 [4], our Gleason 6 versus 9 ES and Staunton et al. Table S1.4 [4], our Gleason 6 versus 9 ES and Tyekucheva et al. Table 2 [5], our Gleason 6 ET versus BE and Sun et al. Table S2A [8], and our Gleason 9 ET versus BE and Sun et al. Table S2A [8]. Immune cell type deconvolution was performed using xCell [18] and ProteoMixture [19]. Fold-change values of differentially enriched xCell signature types in Gleason 6 versus Gleason 9 samples were calculated using Welch's two sample t-test.

Results

LMD enriched TME subpopulations exhibit Gleason score-specific molecular profiles

Surgically-resected formalin-fixed paraffin-embedded (FFPE) prostate tissue specimens from patients with high (Gleason 9; n = 15 specimens from n = 15 patients) or low-grade (Gleason 3 + 3 = 6; n = 23 specimens from n = 15 patients) PCa were serially sectioned to support LMD enrichment of tumor epithelium (ET; n = 34 unique LMD samples), benign epithelium (BE; n = 21), tumor-involved stroma (ES; n = 28), and benign stroma (BS; n = 34) for LC–MS/MS analysis (Fig. 1, Supplemental Table 1). A total of 8,010 and 6,326 proteins were measured in the epithelial and stromal multiplexes, respectively, from which 6,818 (Supplemental Table 2) and 4,685 (Supplemental Table 3) proteins were co-quantified across all epithelial or stromal samples.

Unsupervised hierarchical cluster analysis revealed independent clustering of ET within both Gleason 6 and Gleason 9 specimens from BE, with one exception (Fig. 2A). Stromal sample (ES and BS) clustering was broadly driven by tumor-involvement, though less stringently (Fig. 2B). Differential analyses (limma adj. $p < 0.05$) of LMD enriched populations from Gleason 6 versus Gleason 9 specimens (Fig. 3A) identified 789 and 1,244 significantly altered proteins in ET (Supplemental Table 4) and ES (Supplemental Table 5), respectively.

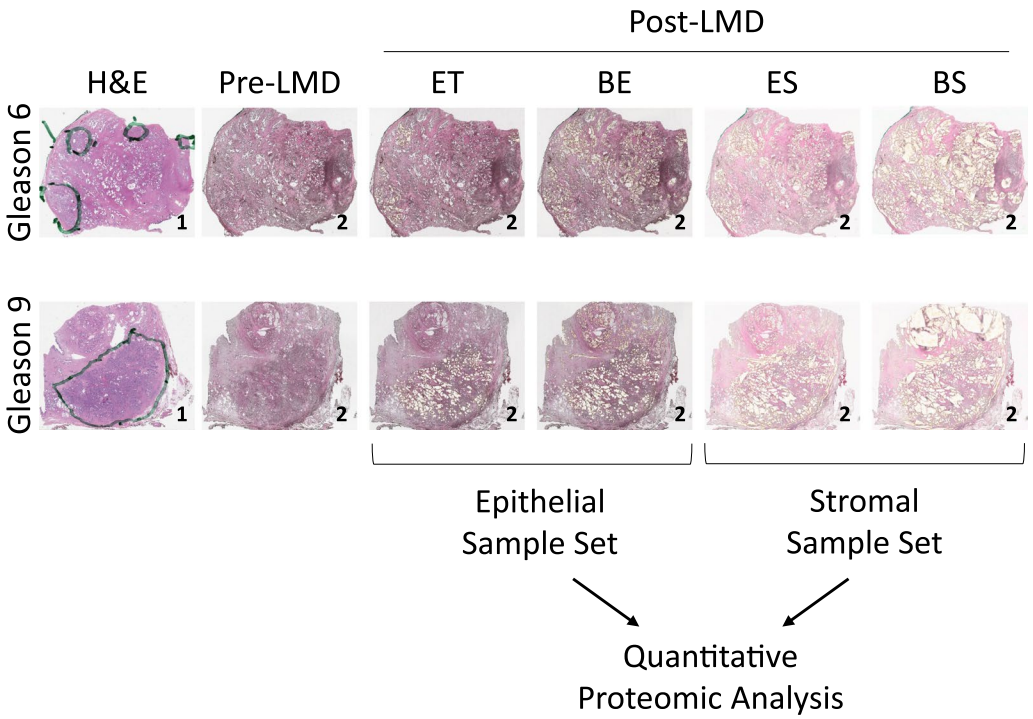

Fig. 1 Workflow diagram. Pre- and post-LMD images of representative Gleason 6 (J4256_461858; top) and Gleason 9 (J4255_461843; bottom) specimens

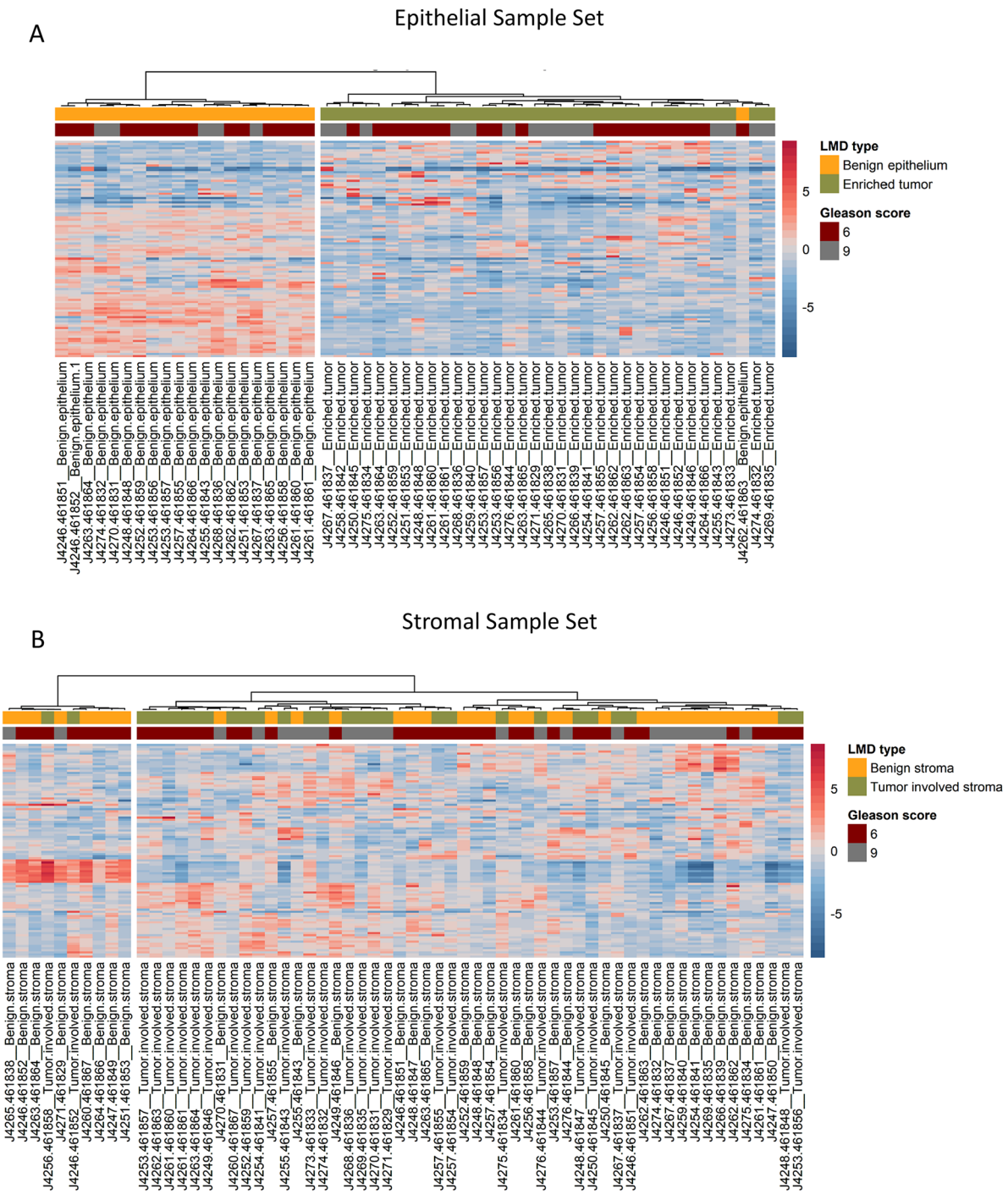

Fig. 2 Unsupervised heatmaps using the most variably abundant proteins (top 100 MAD) in the **A** epithelial (ET and BE) and **B** stromal (ES and BS) samples

Only two significantly altered proteins (PDZ and LIM domain protein 1 (PDLIM1) and polypeptide N-acetylgalactosaminyltransferase 12 (GALNT12)) were measured in the BE from Gleason 6 versus Gleason 9 samples. No significantly altered proteins were measured in the BS of Gleason 6 versus Gleason 9 samples.

The tumor-related specificity of proteomic alterations was examined by comparing tumor-involved versus benign subpopulations enriched from epithelium and

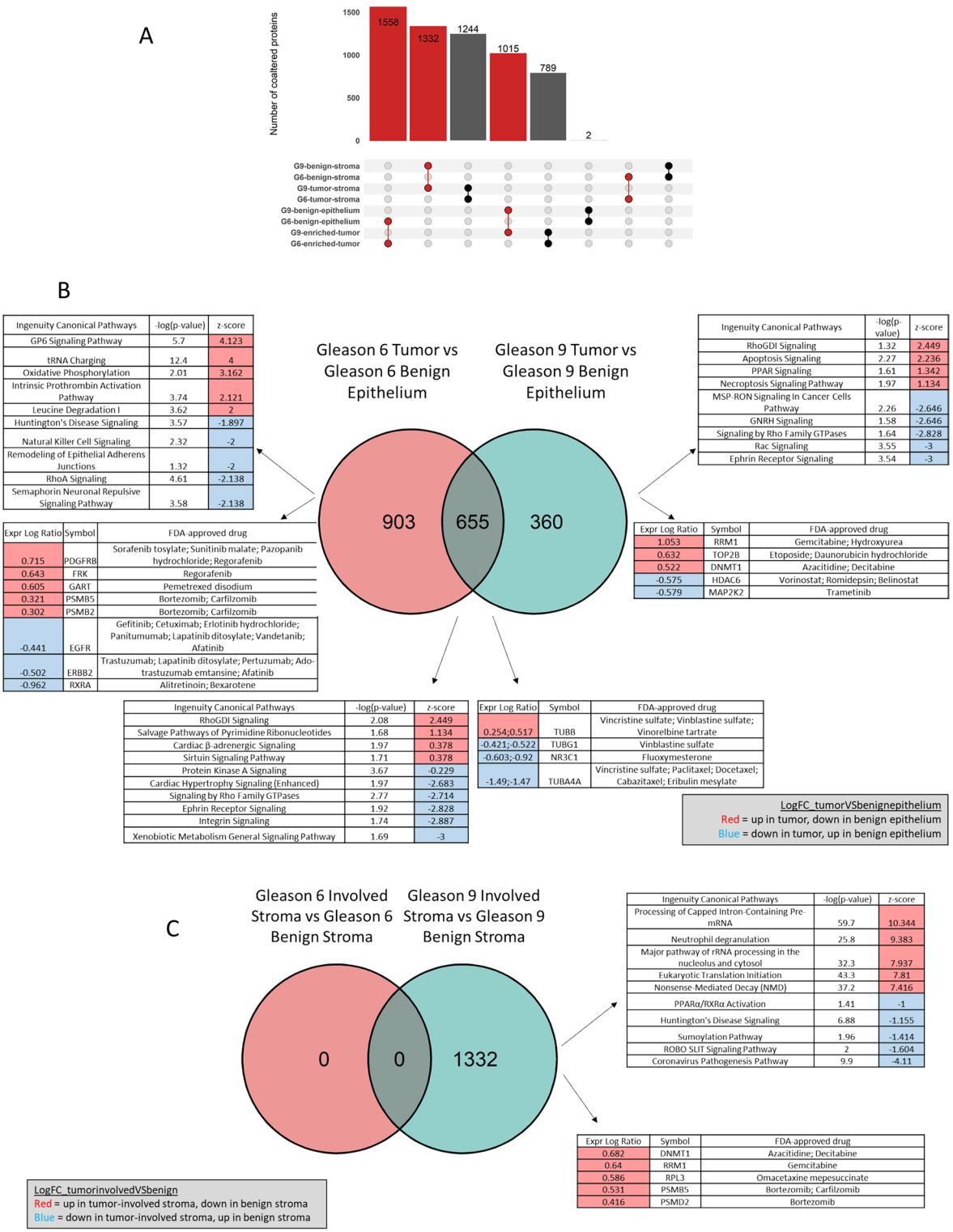

Fig. 3 Differential analyses (limma adj. $p < 0.05$) of LMD enriched sample populations from PCa tissue specimens. **A** Pairwise limma analyses of proteomic abundances from LMD enriched samples. **B** The top five (by z-score) IPA canonical pathways and FDA-approved drug targets identified using differentially abundant proteins between Gleason 6 BE versus Gleason 6 ET, and from Gleason 9 BE versus Gleason 9 ET. **C** The top five IPA canonical pathways and FDA-approved drug targets identified using differentially abundant proteins between Gleason 6 ES versus Gleason 6 BS, and from Gleason 9 ES versus Gleason 9 BS. Pairwise differential analyses used for the (**B**) epithelial and (**C**) stromal comparative analyses are colored red in the upset plot (**A**)

stroma. A total of 1,558 and 1,015 significantly altered proteins (Fig. 3A) were measured in the ET versus BE of Gleason 6 (Supplemental Table 6) and Gleason 9 (Supplemental Table 7) samples, respectively. No significant alterations were measured between Gleason 6 ES versus BS, while 1,332 significantly altered proteins were measured in Gleason 9 ES versus BS (Supplemental Table 8).

Comparative analysis revealed 903 and 360 proteins which were significantly altered in ET versus BE exclusively in Gleason 6 or Gleason 9 samples, respectively, while 655 proteins were co-altered between ET and BE in both grades. Pathway analysis identified the greatest enrichment in RhoGDI signaling, apoptosis signaling, PPAR signaling, and necroptosis signaling in Gleason 9 ET relative to Gleason 9 BE (Fig. 3B, Supplemental Table 9). Comparatively, GP6 signaling, tRNA charging, oxidative phosphorylation, intrinsic prothrombin activation, and leucine degradation were enriched in Gleason 6 ET relative to Gleason 6 BE. Pathways elevated in both the Gleason 6 and Gleason 9 ET (relative to their respective BE) included RhoGDI signaling, salvage pathways of pyrimidine ribonucleotides, cardiac β-adrenergic signaling, and sirtuin signaling.

Gleason 9 ET (relative to Gleason 9 BE) had elevated abundance of proteins representing FDA-approved therapeutic targets [17] (either directly or indirectly through cytotoxic activity) of azacitidine, daunorubicin hydrochloride, decitabine, etoposide, gemcitabine, and hydroxyurea (Fig. 3B, Supplemental Table 10). Gleason 6 ET (relative to Gleason 6 BE) had elevated abundance of FDA-approved targets of bortezomib, carfilzomib, pazopanib hydrochloride, pemetrexed disodium, regorafenib, sorafenib tosylate, and sunitinib malate. TUBB, targeted by vincristine sulfate, vinblastine sulfate, and vinorelbine tartrate, was commonly elevated in the ET of both Gleason 9 and 6 samples (Fig. 3B, Supplemental Table 10).

Tumor-involved stroma from Gleason 9 specimens has unique significance in disease development and/or progression

While substantial grade-specific epithelial alterations existed, 1332 significantly altered proteins between ES and BS were unique to Gleason 9 (and not altered in Gleason 6) (Fig. 3A, C). The most enriched pathways in Gleason 9 ES relative to BS included processing of capped intron-containing pre-mRNA, neutrophil degranulation, major pathway of rRNA processing in the nucleolus and cytosol, eukaryotic translation initiation, and nonsense-mediated decay (NMD) (Fig. 3C, Supplemental Table 9). The most enriched pathways unique to the Gleason 9 BS included coronavirus pathogenesis (largely through quantification of COPI coatomer complex proteins involved in intracellular retrograde transport from the Golgi apparatus to the endoplasmic reticulum), ROBO SLIT signaling, sumoylation pathway, Huntington's disease signaling, and PPARα/RXRα activation. Proteins targeted directly and/or indirectly by azacitidine, decitabine, omacetaxine mepesuccinate, gemcitabine, and hydroxyurea were uniquely enriched in the Gleason 9 ES, but not enriched in Gleason 6 ES or the BS from either grade (Fig. 3C, Supplemental Table 10).

Given the known significance of cholesterol biosynthesis in PCa disease [7], we examined the abundance of cholesterol pathway-related proteins in our LMD enriched samples and identified several were enriched in Gleason 9 ES relative to BS (Fig. 4A, Supplemental Table 9). Comparatively, in the epithelial compartments, cholesterol biosynthetic pathways were elevated in the BE of both Gleason 9 and Gleason 6 cases relative to their respective ET.

Several pathways relating to pyramidine and purine de novo biosynthesis were enriched in Gleason 9 ES relative to BS, while only the salvage pathway of pyramidine ribonucleotides (and no pathways involved in de novo synthesis) was enriched in Gleason 9 ET relative to BE (Fig. 4B, Supplemental Table 9). Comparatively, pathways relating to nucleotide metabolism and/or salvage were enriched in Gleason 6 ET relative to BE.

Correlation of molecular alterations in LMD enriched samples and historical study precedents

Proteomic alterations observed in our datasets correlated positively with study precedents [4, 5] investigating proteomic and/or transcriptomic signatures of LMD enriched cellular subpopulations (Supplemental Fig. 1). Proteins significantly co-altered in our samples and similar analyses of LMD enriched PCa tissue specimens by Staunton et al. [4] were strongly positively correlated (Spearman $\rho = 0.724$, $p < 0.001$) when comparing Gleason 6 ET versus Gleason 9 ET. Comparison of Gleason 6 versus Gleason 9 ES in our dataset against the Staunton [4] dataset showed positive correlation (Spearman $\rho = 0.285$, $p = 0.015$), while a similar comparison using data by Tyekucheva et al. [5] was negatively correlated (Spearman $\rho = -0.586$, $p = 0.015$), likely owing to fewer co-quantified protein-transcript pairs. Alterations between ET and BE were strongly correlated with those in Sun et al. [8] for Gleason 9 specimens (Spearman $\rho = 0.874$, $p < 0.001$), but not correlated for Gleason 6 (Spearman $\rho = 0.005$, $p = 0.993$), suggesting that their PPS1/PPS2 signatures only performed well in our high-grade specimens after LMD enrichment of tumor epithelium.

Immune infiltration differences in TME subpopulations

Immune infiltration into prostate tumors primarily involves quiescent immune populations which do not

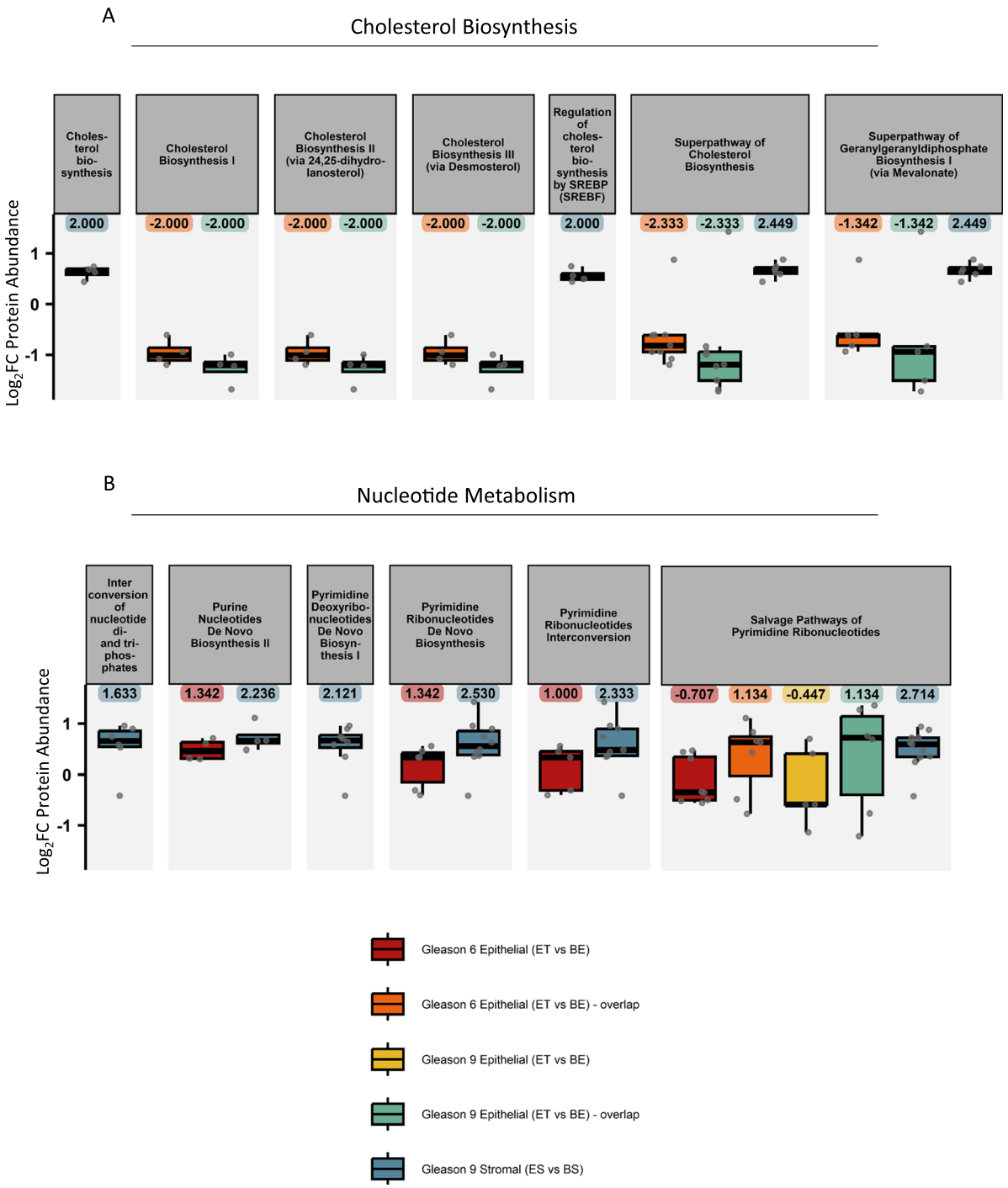

Fig. 4 Boxplots depicting enrichment of IPA canonical pathways relating to **A** cholesterol biosynthesis and **B** nucleotide metabolism. The plots represent the differential analysis $\log_2$-transformed FC values for each pathway-related protein in the notated subsets from comparative analysis. The highlighted number above each box-and-whisker plot represents the IPA z-score for pathway activation. Positive z-scores are enriched in the first LMD cell type comparator (i.e. ET or ES). Negative z-scores are enriched in the second LMD cell type comparator (i.e. BE or BS). Analysis was performed using proteins passing limma adj. $p < 0.05$ and selected IPA pathways passing $p < 0.05$

become activated, with the exception of tumor-promoting M2 macrophages, activated mast cells, and neutrophils, and occurs in a Gleason score-dependent manner [20]. We therefore examined the performance of transcript-derived xCell [18] and protein-derived ProteoMixture [19] signatures for characterizing the immune infiltration in our LMD enriched samples (Fig. 5). Of the 10,808 xCell signature genes, 4,992 (46.2%) and 3,628 (33.6%) were measured at the proteomic level in the LMD enriched epithelial and stromal samples, respectively. A total of 25 unique xCell signatures had grade-specific alterations ($p < 0.05$) in at least one sample type. In concordance with prior studies, most differentially abundant immune populations were elevated in LMD enriched collections from Gleason 6 tissues relative to Gleason 9. CD8 + naïve T cells, Th2 cells, endothelial cells, and microvascular endothelial cells were significantly elevated in the Gleason 9 ET. Th1 cells, class-switched memory B cells, and CD4 + memory T cells were elevated in the Gleason 9 ES. Proportionally higher coverage of the ProteoMixture immune signature was achieved with 242/268 (90.3%) and 210/268 (78.4%) signature proteins quantified in the epithelial and stromal samples, respectively. The median ProteoMixture immune scores in the epithelial and stromal samples were 367 (range = -207 to 1,192) and 213 (range = -314 to 1,321), respectively, representing overall low levels of immune cell infiltrate within the LMD enriched samples.

Tumor epithelial expression of proteins relating to steroid hormone pathways

Androgen deprivation therapy (ADT) is the primary treatment for patients with advanced PCa [21], targeting the aberrant activation of androgen signaling and related steroid hormone metabolic pathways which contribute to the dysregulated proliferation of the tumor [22]. Given the importance of androgen signaling in PCa pathogenesis, we performed a focused analysis of proteins relating to androgen receptor (AR) signaling, androgen metabolism and biosynthesis, and CYP450 family proteins [22–24]. AR, TMPRSS2, MTOR, RPS6KB1, EIF4E, EIF4EBP1, and TSC2 were quantified in ET from Gleason 6 and 9 specimens (Supplemental Table 2), though their abundances were not grade-specific (all $p > 0.05$). SRD5A2 was significantly enriched in the ES from Gleason 6 specimens relative to Gleason 9 (limma adj. $p < 0.05$; Supplemental Table 5). Loss of CYP27A1 in PCa leads to dysregulated cholesterol homeostasis and correlates with shorter disease-free survival and higher Gleason score [25]. Concordantly, significantly lower CYP27A1 abundance was measured in Gleason 9 ET relative to Gleason 6 ET (limma adj. $p < 0.05$; Supplemental Table 4).

Discussion

This study represents a deep proteomic characterization of enriched epithelial and stromal subpopulations from the TME of high- and low-grade PCa tumors. Proteome alterations in our LMD enriched samples correlated positively with previous studies [4, 5, 7]. Benign cellular subpopulations (BE and BS) did not exhibit significant alterations between Gleason 6 versus 9 samples; instead, the grade-specific differences between Gleason 6 versus 9 tumors were exclusive to the TME (ET and ES).

Differential analysis revealed 1,332 proteins exclusively altered between Gleason 9 ES and BS, and not Gleason 6 ES and BS, suggesting that ES from Gleason 9 tumors uniquely contributes to disease development, progression, and/or aggressiveness. Grade-specific stromal enrichment of genes relating to cholesterol homeostasis in PCa tumors was previously measured at the transcript-level [7]. We similarly demonstrate protein-level stromal enrichment of cholesterol biosynthesis from Gleason 9 specimens. Statin use in PCa patients correlates with reduced mortality, Gleason grade, and/or prolonged time to progression [26–30], though some evidence suggests that the benefit of statins may be specific to PCa patients receiving ADT [31, 32], likely owing to the role of cholesterol as a precursor for steroid hormone synthesis.

Several mechanisms describing how cholesterol contributes to PCa disease have been proposed [33–36]. One model demonstrated that the import of extracellular cholesterol into the cytoplasm via low density lipoprotein receptor (LDLR) [33] and further influx of cytoplasmic cholesterol into the nucleus correlates with increased cyclin E expression (34) and tumor cell proliferation [35]. The high bioavailability of cholesterol synthesized in the Gleason 9 stroma may therefore represent a stimulus for PCa tumor cell division. As cholesterol becomes imported from the stroma, tumor cell cyclin E levels increase [34] causing entry into the S-phase of the cell cycle [36]. Collectively, our data provide supportive evidence of a need for further investigations into concurrent clinical administration of ADT and statins in PCa patients for reducing stromal cholesterol pools, with independent proteomic analysis of the TME epithelial and stromal compartments.

Several pathways relating to de novo biosynthesis of nucleotides (an energy-intensive process) were exclusively enriched in Gleason 6 ET relative to Gleason 6 BE, while not also enriched in Gleason 9 ET relative to Gleason 9 BE. Comparatively, de novo synthetic pathways were instead enriched in Gleason 9 ES relative to BS. Only pyrimidine ribonucleotide salvage pathways, which are more energy-efficient, were enriched in Gleason 9 ET. The salvage pathway was not exclusive to the Gleason 9 ET as it was further identified using additional

A

LMD Enriched Tissue	xCell Signature Population	FC	P-value	Elevated In	% Coverage
Tumor Epithelium (ET)	Platelets	17.384	0.021	Gleason 6	37.4
	CD4+ Tcm	5.733	0.03	Gleason 6	51.5
	Macrophages	4.762	0.002	Gleason 6	56
	Epithelial cells	2.45	0.015	Gleason 6	52.7
	CD8+ naive T-cells	0.605	0.032	Gleason 9	38.5
	Th2 cells	0.479	0.04	Gleason 9	40.9
	Endothelial cells	0.384	0.038	Gleason 9	58
	mv Endothelial cells	0.306	0.011	Gleason 9	61
Benign Epithelium (BE)	Hepatocytes	1.09E+16	0.003	Gleason 6	39.8
	Pericytes	4.27E+15	0.039	Gleason 6	56.7
	B-cells	4.11E+15	0.022	Gleason 6	34.8
	Myocytes	4.71E+03	0.012	Gleason 6	60.5
	Th2 cells	33.518	0.012	Gleason 6	40.9
	pro B-cells	9.521	0.017	Gleason 6	24.7
	Neurons	8.392	0.013	Gleason 6	22.7
	Epithelial cells	0.813	0.018	Gleason 9	52.7
	HSC	0.52	0.005	Gleason 9	30
Tumor-Involved Stroma (ES)	DC	51.977	0.001	Gleason 6	33
	Astrocytes	34.186	0.026	Gleason 6	41.1
	Th2 cells	4.262	0.045	Gleason 6	40.9
	iDC	3.074	0.021	Gleason 6	21.4
	Th1 cells	0.445	0.037	Gleason 9	61.1
	Class-switched memory B-cells	0.441	0.028	Gleason 9	50
	CD4+ memory T-cells	0.219	0.037	Gleason 9	72.4
Benign Stroma (BS)	Memory B-cells	3.864	0.033	Gleason 6	13.6
	Macrophages M2	3.544	0.032	Gleason 6	55.3
	Epithelial cells	2.801	0.016	Gleason 6	52.7
	Sebocytes	2.769	0.043	Gleason 6	34.3
	MEP	1.899	0.039	Gleason 6	65.7

B

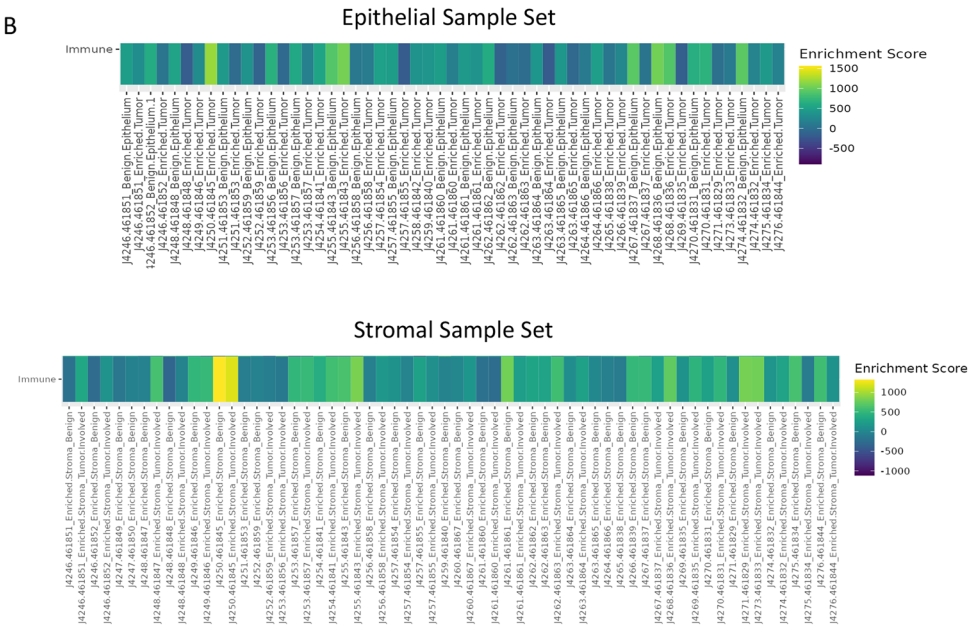

Fig. 5 Characterization of immune cell signatures in LMD enriched PCa samples. **A** xCell [18] immune cell types significantly differing (Welch's two sample t-test $p < 0.05$) in TME cellular subpopulations from Gleason 6 versus Gleason 9 specimens. FC = fold change. % Coverage = the percentage of marker genes in the xCell cell type signature which were measured at the proteomic level in LMD enriched samples. **B** ProteoMixture immune scores of LMD enriched epithelial (top) and stromal (bottom) samples

subsets of pathway-related proteins in the ET and/or ES of Gleason 6 and Gleason 9 cases, likely indicating that all TME subpopulations rely to some degree on the availability and conversion of endogenous salvaged bases from natural nucleic acid turnover and/or dietary supplementation. Collectively, these data suggest that the

Gleason 9 tumor cells may rely on the salvage of stromal deoxynucleoside triphosphate (dNTP) reservoirs to meet replication requirements [37]. Nucleotide deficiency contributes to replication stress and DNA damage [38–42], which are patho-genomic characteristics of advanced PCa. Degradation of pyrimidines promotes epithelial-to-mesenchymal transition (EMT) [43, 44]. Spindle-shaped mesenchymal tumor cells are a morphological characteristic of advanced PCa [45]. The FDA-approved direct and/or indirect targets [17] of gemcitabine, decitabine, and azacytidine (which interfere with the incorporation of nucleotides into DNA [46, 47]) were enriched in both Gleason 9 ET and ES. Future studies should examine the clinical efficacy of drugs targeting stromal dNTP reservoirs as well as nucleotide salvage pathway mediators in the tumor cells [48], with additional considerations when examining the combinatorial use of chemotherapy and immunotherapy in PCa. Interestingly, alterations in DNA metabolism are correlated with clinical response to neoadjuvant chemotherapy (NACT) in HGSOC patients; as patients who were excellent responders had higher enrichment of proteins relating to DNA metabolism [14], including elevation of several of the relevant pathway-related proteins quantified here.

ADT remains the primary treatment for patients with advanced PCa [21]. While several proteins involved in androgen metabolism and/or biosynthesis were quantified in the ET of both Gleason 6 and Gleason 9, their abundances were not grade-specific. The enrichment of CD8 + naïve T cell and Th2 cell signatures in Gleason 9 ET, and CD4 + memory T cell and Th1 cell signatures in Gleason 9 ES support a positive role for T cell-promoting immunotherapies, in agreement with previous clinical trials. Three FDA-approved immunotherapy options are available for qualifying patients with advanced stage PCa. Sipuleucel-T is an autologous vaccine which targets prostatic acid phosphatase and promotes activation of antigen presenting cells and CD8 + T cells [49, 50]. Pembrolizumab and dostarlimab are monoclonal antibodies for immune checkpoint inhibition and improve T cell activation [51, 52].

Conclusions

Collectively, we demonstrate grade-specific alterations in both the epithelial and stromal compartments of PCa tumors, with many exclusive alterations in Gleason 9 ES. While some of these observations have been previously described in vitro or at the transcript-level, the quantification of grade-specific protein-level alterations in distinct cellular compartments of the TME highlights the necessity for upfront sample processing and LMD enrichment, as disease-relevant PCa contributors are present in both tumor epithelium and stroma.

Abbreviations

ADT	Androgen deprivation therapy
AR	Androgen receptor
BE	Enriched benign epithelium
bRPLC	Basic reversed-phase liquid chromatography
BS	Enriched benign stroma
dNTP	Deoxynucleoside triphosphate
EMT	Epithelial-to-mesenchymal transition
ES	Enriched tumor-involved stroma
ET	Enriched tumor
FFPE	Formalin-fixed paraffin-embedded
GALNT12	Polypeptide N-acetylgalactosaminyltransferase 12
GG	Gleason Grade Group
H&E	Hematoxylin and eosin
IPA	Ingenuity Pathway Analysis
ISUP	International Society of Urological Pathology
LC–MS/MS	Liquid chromatography tandem mass spectrometry
LDLR	Low density lipoprotein receptor
LMD	Laser microdissection
MAD	Median absolute deviation
NACT	Neoadjuvant chemotherapy
NMD	Nonsense-mediated decay
PCa	Prostate cancer
PDLIM1	PDZ and LIM domain protein 1
PEN	Polyethylene napthalate
PSA	Prostate specific antigen
TME	Tumor microenvironment
TNM	American Joint Commission on Cancer TNM system for classification of malignant tumors
TMT	Tandem mass tag

Supplementary Information

The online version contains supplementary material available at https://doi.org/10.1186/s12014-025-09534-8.

Additional file 1.

Additional file 2.

Acknowledgements

This work was supported, in part, by funds from the Inova Schar Cancer Institute. The authors would like to acknowledge Dr. Uma Rao for histopathology analysis support, and Persus Akowuah and Jeremy Loffredo for proteomic sample preparation support.

Disclaimer

The views expressed in this article are those of the author(s) and do not necessarily reflect the official policy or position of the Uniformed Services University of the Health Sciences (USUHS), Department of the Navy, Department of the Air Force, Department of the Army, Department of Defense, or the United States Government. Mention of trade names, commercial products, or organizations does not imply endorsement by the U.S. Government.

Author contributions

Contributed to conception: T.P.C and D.L.T. Contributed to experimental design: T.P.C., N.W.B., and A.L.H. Contributed to identification and acquisition of the patient specimens: D.L.T. and H.M. Contributed to acquisition, analysis, and/or interpretation of data: A.L.H., W.B., S.C.M-M., B.L.H., K.A.C., K.N.W., T.A., J.O., K.J.P., T.L.L., H.M., D.L.T., N.W.B., and T.P.C. Drafted and/or revised the manuscript: A.L.H., N.W.B., D.L.T., and T.P.C. All authors read and approved the final manuscript.

Funding

This work was supported, in part, by funds from the Inova Schar Cancer Institute.

Data availability
The mass spectrometry proteomic data have been deposited to the ProteomeXchange Consortium via the PRIDE partner repository [53] with the dataset identifier PXD058689.

Declarations

Ethics approval and consent to participate
Archival formalin-fixed paraffin embedded (FFPE) tissues were obtained from an IRB-approved protocol (#12–1169, 20122048) from Inova Fairfax Medical Campus (Falls Church, VA, USA). All experimental protocols involving human data in this study were in accordance with the Declaration of Helsinki.

Consent for publication
WIRB-Copernicus Group Institutional Review Board (WCG IRB) approved this study. All participants provided written informed consent. The written informed consent included the provision to analyze and publish information and data regarding the results and data from molecular testing, such as proteomics and nucleic acid sequencing.

Competing interests
T.P.C. is a ThermoFisher Scientific, Inc. SAB member and receives research funding from AbbVie.

Author details
[1]Women's Health Integrated Research Center, Inova Women's Service Line, Inova Health System, 3289 Woodburn Rd, Annandale, VA 22003, USA. [2]Gynecologic Cancer Center of Excellence and the Women's Health Integrated Research Center, Department of Gynecologic Surgery and Obstetrics, Uniformed Services University and Walter Reed National Military Medical Center, 8901 Wisconsin Avenue, Bethesda, MD 20889, USA. [3]The Henry M. Jackson Foundation for the Advancement of Military Medicine, Inc, 6720A Rockledge Drive, Suite 100, Bethesda, MD 20817, USA. [4]The John P. Murtha Cancer Center Research Program, Department of Surgery, Uniformed Services University, 8901 Wisconsin Avenue, Bethesda, MD 20889, USA. [5]The Brady Urological Institute, Johns Hopkins School of Medicine, Baltimore, MD, USA. [6]Department of Pathology, Johns Hopkins School of Medicine, Baltimore, MD, USA. [7]Department of Oncology, Sidney Kimmel Comprehensive Cancer Center, Johns Hopkins University School of Medicine, Baltimore, MD, USA. [8]Department of Urology, Johns Hopkins University School of Medicine, Baltimore, MD, USA. [9]Department of Pathology, Inova Fairfax Hospital, 3300 Gallows Road, Falls Church, VA 22042, USA. [10]Inova Schar Cancer Institute, Inova Health System, 8081 Innovation Park Dr, Fairfax, VA 22031, USA.

Received: 18 December 2024 Accepted: 19 March 2025
Published online: 20 April 2025

References

1. Siegel RL, Kratzer TB, Giaquinto AN, Sung H, Jemal A. Cancer statistics, 2025. CA A Cancer J Clin. 2025;75(1):10–45.
2. Network NCC. Prostate cancer (version 2.2023). 2023. https://www.nccn.org/guidelines/guidelines-detail?category=1&id=1459.
3. Epstein JI, Egevad L, Amin MB, Delahunt B, Srigley JR, Humphrey PA. The 2014 International society of urological pathology (ISUP) consensus conference on gleason grading of prostatic carcinoma: definition of grading patterns and proposal for a new grading system. Am J Surg Pathol. 2016;40(2):244–52.
4. Staunton L, Tonry C, Lis R, Espina V, Liotta L, Inzitari R, et al. Pathology-driven comprehensive proteomic profiling of the prostate cancer tumor microenvironment. Mol Cancer Res. 2017;15(3):281–93.
5. Tyekucheva S, Bowden M, Bango C, Giunchi F, Huang Y, Zhou C, et al. Stromal and epithelial transcriptional map of initiation progression and metastatic potential of human prostate cancer. Nat Commun. 2017;8(1):420.
6. Georgescu I, Gooding RJ, Doiron RC, Day A, Selvarajah S, Davidson C, et al. Molecular characterization of Gleason patterns 3 and 4 prostate cancer using reverse Warburg effect-associated genes. Cancer Metab. 2016;4(1):8.
7. Ma C, Zhou Y, Fanelli GN, Stopsack KH, Fiorentino M, Zadra G, et al. The prostate stromal transcriptome in aggressive and lethal prostate cancer. Mol Cancer Res. 2023;21(3):253–60.
8. Sun R, Tan L, Ding X, Xue Z, Cai X, et al. A pathway activity-based proteomic classifier stratifies prostate tumors into two subtypes. Clin Proteomics. 2023;20(1):50.
9. Silva MM, Matheus WE, Garcia PV, Stopiglia RM, Billis A, Ferreira U, Fávaro WJ, et al. Characterization of reactive stroma in prostate cancer: involvement of growth factors, metalloproteinase matrix, sexual hormones receptors and prostatic stem cells. Int Braz J Urol. 2015;41(5):849–58.
10. Saeter T, Vlatkovic L, Waaler G, Servoll E, Nesland JM, Axcrona K, et al. The prognostic value of reactive stroma on prostate needle biopsy: a population-based study. Prostate. 2015;75(6):662–71.
11. Ruder S, Gao Y, Ding Y, Bu P, Miles B, De Marzo A, et al. Development and validation of a quantitative reactive stroma biomarker (qRS) for prostate cancer prognosis. Hum Pathol. 2022;122:84–91.
12. Levesque C, Nelson PS. Cellular constituents of the prostate stroma: key contributors to prostate cancer progression and therapy resistance. Cold Spring Harb Perspect Med. 2018;8(8): a030510.
13. Tuxhorn JA, Ayala GE, Smith MJ, Smith VC, Dang TD, Rowley DR. Reactive stroma in human prostate cancer: induction of myofibroblast phenotype and extracellular matrix remodeling. Clin Cancer Res. 2002;8(9):2912–23.
14. Lee S, Zhao L, Rojas C, Bateman NW, Yao H, Lara OD, et al. Molecular analysis of clinically defined subsets of high-grade serous ovarian cancer. Cell Rep. 2020;31(2): 107502.
15. Bateman NW, Tarney CM, Abulez TS, Hood BL, Conrads KA, Zhou M, et al. Peptide ancestry informative markers in uterine neoplasms from women of European, African, and Asian ancestry. iScience. 2022;25(1):103665.
16. Ritchie ME, Phipson B, Wu D, Hu Y, Law CW, Shi W, et al. limma powers differential expression analyses for RNA-sequencing and microarray studies. Nucleic Acids Res. 2015;43(7):47.
17. Sun J, Wei Q, Zhou Y, Wang J, Liu Q, Xu H. A systematic analysis of FDA-approved anticancer drugs. BMC Syst Biol. 2017;11(Suppl 5):27–43.
18. Aran D, Hu Z, Butte AJ. xCell: digitally portraying the tissue cellular heterogeneity landscape. Genome Biol. 2017;18(1):220.
19. Teng PN, Schaaf JP, Abulez T, Hood BL, Wilson KN, Litzi TJ, et al. ProteoMixture: a cell type deconvolution tool for bulk tissue proteomics data. BioRxiv. 2023;244:628.
20. Wu Z, Chen H, Luo W, Zhang H, Li G, Zeng F, et al. The landscape of immune cells infiltrating in prostate cancer. Front Oncol. 2020;10:517637.
21. Sharifi N, Gulley JL, Dahut WL. Androgen deprivation therapy for prostate cancer. JAMA. 2005;294(2):238–44.
22. Culig Z, Santer FR. Androgen receptor signaling in prostate cancer. Cancer Metastasis Rev. 2014;33(2):413–27.
23. Reid AH, Attard G, Barrie E, de Bono JS. CYP17 inhibition as a hormonal strategy for prostate cancer. Nat Clin Pract Urol. 2008;5(11):610–20.
24. Chen TC, Sakaki T, Yamamoto K, Kittaka A. The Roles of cytochrome P450 enzymes in prostate cancer development and treatment. Anticancer Res. 2012;32(1):291–8.
25. Alfaqih MA, Nelson ER, Liu W, Safi R, Jasper JS, Macias E, et al. CYP27A1 loss dysregulates cholesterol homeostasis in prostate cancer. Cancer Res. 2017;77(7):1662–73.
26. Harshman LC, Wang X, Nakabayashi M, Xie W, Valenca L, Werner L, et al. Statin use at the time of initiation of androgen deprivation therapy and time to progression in patients with hormone-sensitive prostate cancer. JAMA Oncol. 2015;1(4):495–504.
27. Yu O, Eberg M, Benayoun S, Aprikian A, Batist G, Suissa S, et al. Use of statins and the risk of death in patients with prostate cancer. J Clin Oncol. 2014;32(1):5–11.
28. Farwell WR, Avolio LW, Scranton RE, Lawler EV, Gaziano JM. Statins and prostate cancer diagnosis and grade in a veterans population. J Natl Cancer Inst. 2011;103(11):885–92.
29. Larsen SB, Dehlendorff C, Skriver C, Dalton SO, Jespersen CG, Borre M, et al. Postdiagnosis statin use and mortality in Danish patients with prostate cancer. J Clin Oncol. 2017;35(29):3290–7.
30. Reilly JE, Neighbors JD, Hohl RJ. Targeting protein geranylgeranylation slows tumor development in a murine model of prostate cancer metastasis. Cancer Biol Ther. 2017;18(11):872–82.

31. Hou YC, Shao YH. The effects of statins on prostate cancer patients receiving androgen deprivation therapy or definitive therapy: a systematic review and meta-analysis. Pharmaceuticals (Basel). 2022;15(2):131.
32. Chan JM, Kenfield SA, Paciorek A, Platz EA, Giovannucci EL, Stampfer MJ. Postdiagnostic statin use and the risk of lethal prostate cancer in the health professionals follow-up study. Cancer Epidemiol Biomark Prev. 2015;24(10):1638–40.
33. Brown MS, Goldstein JL. Receptor-mediated endocytosis: insights from the lipoprotein receptor system. Proc Natl Acad Sci USA. 1979;76(7):3330–7.
34. Singh G, Sankanagoudar S, Dogra P, Chandra NC. Interlink between cholesterol and cell cycle in prostate carcinoma. Indian J Med Res. 2017;146(Suppl):S38–44.
35. Raftopulos NL, Washaya TC, Niederprüm A, Egert A, Hakeem-Sanni MF, Varney B, et al. Prostate cancer cell proliferation is influenced by LDL-cholesterol availability and cholesteryl ester turnover. Cancer Metab. 2022;10(1):1.
36. Lundberg AS, Weinberg RA. Functional inactivation of the retinoblastoma protein requires sequential modification by at least two distinct cyclin-cdk complexes. Mol Cell Biol. 1998;18(2):753–61.
37. Wang Q, Guan YF, Hancock SE, Wahi K, van Geldermalsen M, Zhang BK, et al. Inhibition of guanosine monophosphate synthetase (GMPS) blocks glutamine metabolism and prostate cancer growth. J Pathol. 2021;254(2):135–46.
38. Huang R-H, Hong Y-K, Du H, Ke W-Q, Lin B-B, Li Y-L. A machine learning framework develops a DNA replication stress model for predicting clinical outcomes and therapeutic vulnerability in primary prostate cancer. J Transl Med. 2023;21(1):20.
39. Austin WR, Armijo AL, Campbell DO, Singh AS, Hsieh T, Nathanson D, et al. Nucleoside salvage pathway kinases regulate hematopoiesis by linking nucleotide metabolism with replication stress. J Exp Med. 2012;209(12):2215–28.
40. Poli J, Tsaponina O, Crabbé L, Keszthelyi A, Pantesco V, Chabes A, et al. dNTP pools determine fork progression and origin usage under replication stress. EMBO J. 2012;31(4):883–94.
41. Pontarin G, Ferraro P, Bee L, Reichard P, Bianchi V. Mammalian ribonucleotide reductase subunit p53R2 is required for mitochondrial DNA replication and DNA repair in quiescent cells. Proc Natl Acad Sci. 2012;109(33):13302–7.
42. D'Angiolella V, Donato V, Forrester Frances M, Jeong Y-T, Pellacani C, Kudo Y, et al. Cyclin F-mediated degradation of ribonucleotide reductase M2 controls genome integrity and DNA repair. Cell. 2012;149(5):1023–34.
43. Shaul YD, Freinkman E, Comb WC, Cantor JR, Tam WL, Thiru P, et al. Dihydropyrimidine accumulation is required for the epithelial-mesenchymal transition. Cell. 2014;158(5):1094–109.
44. Siddiqui A, Gollavilli PN, Schwab A, Vazakidou ME, Ersan PG, Ramakrishnan M, et al. Thymidylate synthase maintains the de-differentiated state of triple negative breast cancers. Cell Death Differ. 2019;26(11):2223–36.
45. Odero-Marah V, Hawsawi O, Henderson V, Sweeney J. Epithelial–mesenchymal transition (EMT) and prostate cancer. Adv Exp Med Biol. 2018;1095:101–10.
46. Plunkett W, Huang P, Xu YZ, Heinemann V, Grunewald R, Gandhi V. Gemcitabine: metabolism, mechanisms of action, and self-potentiation. Semin Oncol. 1995;22(4 Suppl 11):3–10.
47. Mullen NJ, Singh PK. Nucleotide metabolism: a pan-cancer metabolic dependency. Nat Rev Cancer. 2023;23(5):275–94.
48. Walter M, Herr P. Re-discovery of pyrimidine salvage as target in cancer therapy. Cells. 2022;11(4):739.
49. Kantoff PW, Higano CS, Shore ND, Berger ER, Small EJ, Penson DF, et al. Sipuleucel-T immunotherapy for castration-resistant prostate cancer. N Engl J Med. 2010;363(5):411–22.
50. Fong L, Carroll P, Weinberg V, Chan S, Lewis J, Corman J, et al. Activated lymphocyte recruitment into the tumor microenvironment following preoperative sipuleucel-T for localized prostate cancer. J Natl Cancer Inst. 2014;106(11):dju268.
51. Reck M, Rodríguez-Abreu D, Robinson AG, Hui R, Csőszi T, Fülöp A, et al. Pembrolizumab versus chemotherapy for PD-L1–positive non–small-cell lung cancer. N Engl J Med. 2016;375(19):1823–33.
52. Oaknin A, Tinker AV, Gilbert L, Samouëlian V, Mathews C, Brown J, et al. Clinical activity and safety of the anti-programmed death 1 monoclonal antibody dostarlimab for patients with recurrent or advanced mismatch repair-deficient endometrial cancer: a nonrandomized phase 1 clinical trial. JAMA Oncol. 2020;6(11):1766–72.
53. Perez-Riverol Y, Csordas A, Bai J, Bernal-Llinares M, Hewapathirana S, Kundu DJ, et al. The PRIDE database and related tools and resources in 2019: improving support for quantification data. Nucleic Acids Res. 2019;47(D1):D442–50.

Publisher's Note